REVIEW OF RECENT DEVELOPMENTS AND FUTURE CHALLENGES FOR THE SIMULATION-BASED DESIGN OF AIRCRAFT

Frédéric Chalot*, Michel Mallet* and Gilbert Rogé*
* Advanced Aerodynamics and Aeroacoustics, Dassault Aviation, Saint Cloud, France

Keywords: *optimization, flutter, DES, aeroacoustics, uncertainties*

Abstract

Efficient and reliable simulation-based processes are essential to the design of innovative and competitive future aircraft. Continued efforts over the past years have lead to impressive progress and new tools. The review presentation will illustrate key issues associated to the following topics: automatic shape optimization, aerodynamic models for aeroelastic analysis, Detached Eddy Simulation (DES) for complex flows and loads, aeroacoustics and uncertainty quantification.

1 Introduction

The objective of the paper is to review a number of key developments in the simulation based design of aircraft. Progress is fast and the scope of the paper is large. Each example will only be briefly addressed.

Reference review papers include a thorough presentation of the status of CFD for aerodynamics by Jameson [1], Chalot [2] and the 100th volume of NNFM [3]. A review of the design methods applied to the Falcon 7X project was presented by Rostand [4].

The paper will first describe the progress of automated design process. The new methods for flutter prediction will than illustrate new multidisciplinary capabilities. Next, Detached Eddy Simulation (DES) for complex flows and loads will demonstrate the impact of unsteady simulations. Finally, the new fields of aeroacoustics and uncertainty quantification will be discussed.

2 Automatic shape optimization

This capability can have a profound impact on the design process, mainly via a huge reduction of the time required for shape definition of a parametrized shape.

2.1 Optimization process

The optimization process is based on an iterative loop that requires the coupling of various modules.

The optimizer module drives the whole process. It relies on gradients. For constrained cases, the preferred approach is the Interior Point Algorithm [5].

A key ingredient is the use of a CAD-based modeler which is described in the next section. Geometric constraints can be treated by this modeler and this contributes to the efficiency of the process.

The aerodynamic response is provided by Euler or Navier-Stokes CFD solvers on unstructured meshes. The cost and constraints are evaluated by a separate cost function tool.

The gradients supplied to the optimizer are evaluated using a discrete adjoint formulation both for the volume mesh deformation and for the aerodynamic state equations. The modeler has also been differentiated.

2.2 Geometric CAD Modeler

The CAD modeler named Ganimede handles both local variables (CAD parameters) and global design variables (geometric "features") [6], [7]. Local design variables include position, tangent and curvature values at

control point level. Global design variables couple several control points to allow a modification of "features" such as thickness, twist and camber of wing sections.

Once a new geometry is defined during the optimization loop, the modified surface mesh must be redefined. This is performed by Ganimede. At the beginning of the process, a connectivity is created by projection of the initial surface mesh on the initial geometry. The new geometry, the connectivity and the topology of the initial mesh are used to generate each new surface mesh. The initial volume mesh is then deformed using the new surface mesh and a Laplacian like operator.

The capacity of the modeler is illustrated in Figure 2.1. In this case both wing twist and camber variables are considered. The CAD is modified and the surface mesh is projected on the new CAD. The initial and modified meshes are presented.
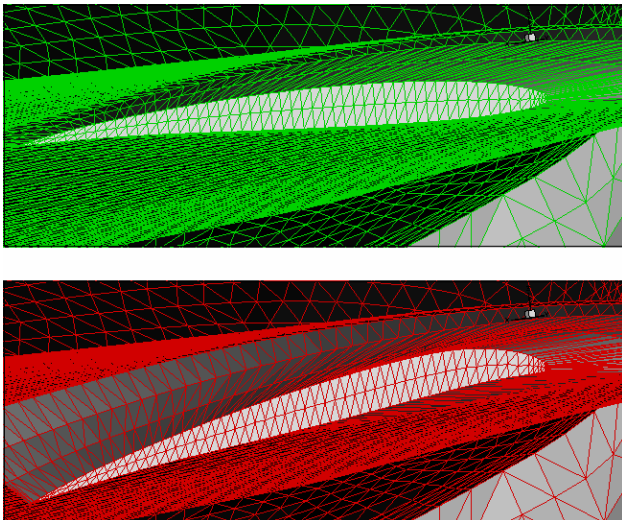

Fig. 2.1: Initial (top) and modified (bottom) surface mesh produced by the geometric modeler when wing twist and camber variables are modified

2.3 Optimization of the shape of a nacelle

The optimization process is illustrated by the optimization of the shape of the nacelle of a Falcon business jet. In this case, we consider the nacelle of the central engine. The nacelle diameter is increased to fit larger engines with increased bypass ratio. The initial design with the modified nacelle generates significant wave drag at high transonic Mach number (Mach =0.88).

The optimization parameters include six CAD variables. Two objective functions have been considered: initially, an inverse problem based on the definition of target pressure distributions on a number of lines along the nacelle was performed; a direct drag minimization was then considered. Both approaches are successful in this case. A slightly better result is obtained with the drag minimization approach, but the initial convergence of the process is faster when the inverse design process is selected.

The adjoint-based optimization typically converges after about 20 optimization cycles.

The initial and optimized designs are illustrated on Figure 2.2. The wave drag of the proposed design is almost zero in the re-designed area.
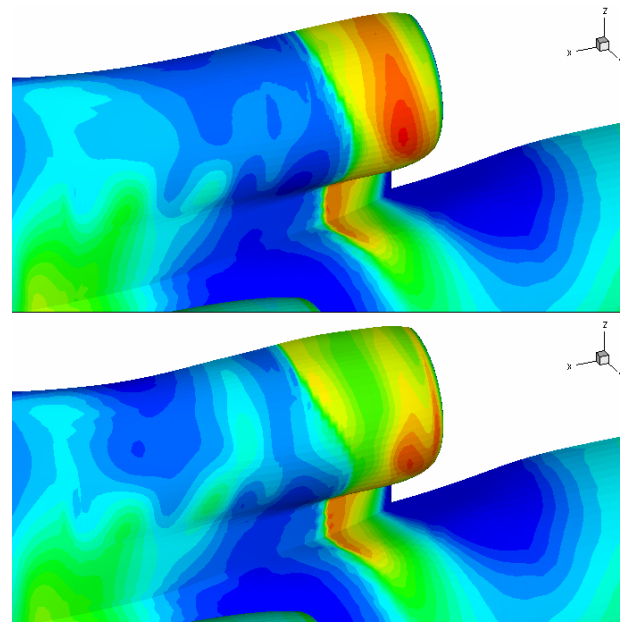

Fig. 2.2 : Pressure coefficient on the initial (top) and optimized (bottom) nacelle shapes.

Optimization procedures are getting more and more mature. Their impact will grow progressively as we gain more experience with various applications and also with the increase in the scope of the modeler, with improved robustness of the solvers and with new objective functions. New tools to compute 2nd order derivatives are emerging (see paragraph 6 and [20]). These tools will most probably have a large impact on the optimization process.

3 Aerodynamic models for aeroelastic analysis

The Doublet Lattice Method (DLM) is the reference tool to produce the aerodynamic data required for flutter prediction in the subsonic regime. However, complex flow features that are typical of transonic flows (shock waves or separated flow), cannot be predicted by the DLM. The prediction of the aerodynamic loads thus requires new methods which can predict more complex flows and also fulfill two requirements:

- Low computational cost which is mandatory because of the very large number of load cases that must be analyzed.
- The ability to deal with complex configurations especially for military applications (Figure 3.1) (weapons integration). This requires the use of CFD codes on unstructured meshes.
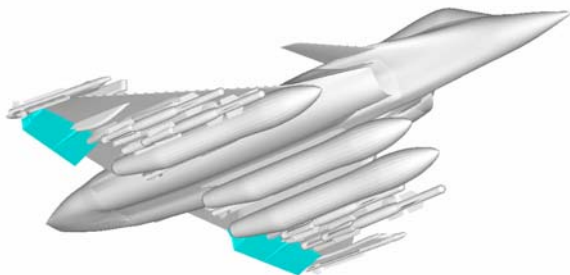
.

Fig. 3.1: Example of a military configuration considered for aeroelastic analysis

A frequency domain linearized Euler and Navier-Stokes approach was selected. The new reference tool relies on the linearized Euler equations [8], it is now well integrated in the aeroelastic design process. More recently, the Navier-Stokes solver has also been linearized [9].

3.1 Linearized Navier-Stokes equations

The Navier-Stokes equations can be written as

$$E(\boldsymbol{V}, \dot{\boldsymbol{V}}, \boldsymbol{x}, \boldsymbol{w}) = 0$$

where $\boldsymbol{V}$ denotes the entropy variables, $\boldsymbol{x}$ the coordinates and $\boldsymbol{w}$ the mesh velocity.
Let us consider a perturbation $d\boldsymbol{x}$ of $\boldsymbol{x}$ around $\boldsymbol{x_0}$ and the resulting perturbed state $d\boldsymbol{V}$ around $\boldsymbol{V_0}$.

Upper dots denote time derivatives. The frequency formulation yields

$$\boldsymbol{x} = \boldsymbol{x}_0 + d\boldsymbol{x}e^{i\omega t} \qquad \boldsymbol{w} = d\boldsymbol{w}e^{i\omega t}$$

$$\boldsymbol{V} = \boldsymbol{V}_0 + d\boldsymbol{V}e^{i\omega t} \qquad \dot{\boldsymbol{V}} = d\dot{\boldsymbol{V}}e^{i\omega t}$$

with $\mathbf{x_0}$ and $\mathbf{V_0}$ satisfying

$$E(\boldsymbol{V}_0, \boldsymbol{0}, \boldsymbol{x}_0, \boldsymbol{0}) = 0$$

and

$$\boldsymbol{w} = \frac{\partial x}{\partial t} = i\omega d\boldsymbol{x}e^{i\omega t} \qquad d\boldsymbol{w} = i\omega d\boldsymbol{x}$$

$$\dot{\boldsymbol{V}} = \frac{\partial \boldsymbol{V}}{\partial t} = i\omega d\boldsymbol{V}e^{i\omega t} \qquad d\dot{\boldsymbol{V}} = i\omega d\boldsymbol{V}$$

The linearization of the Navier Stokes equation gives to first order:

$$dE = \frac{\partial E}{\partial \boldsymbol{V}}d\boldsymbol{V} + \frac{\partial E}{\partial \dot{\boldsymbol{V}}}d\dot{\boldsymbol{V}} + \frac{\partial E}{\partial \boldsymbol{x}}d\boldsymbol{x} + \frac{\partial E}{\partial \boldsymbol{w}}d\boldsymbol{w} = 0$$

Thus the complex variation $d\boldsymbol{V}$ of the entropy variables can be generated by resolving

$$\left(\frac{\partial E}{\partial \boldsymbol{V}} + i\omega\frac{\partial E}{\partial \dot{\boldsymbol{V}}}\right)d\boldsymbol{V} = -\left(\frac{\partial E}{\partial \boldsymbol{x}}\right)d\boldsymbol{x} - i\omega\left(\frac{\partial E}{\partial \boldsymbol{w}}\right)$$

All the operators appearing in the above equation have been obtained using an Automatic Differentiation tool called Tapenade developed by INRIA Sophia Antipolis [10]. This tool provides the differentiated Fortran routines with respect to input variables prescribed by the user.

3.2 Wing/body configuration in transonic flow

An industrial validation test case was performed in the transonic regime. The selected wing/body configuration is presented below

Fig. 3.2: Nonlinear flutter model

The wing structure was designed to exhibit a typical flutter case involving a coupling between wing bending and torsion modes. The experiment was carried out in the ONERA S2MA transonic wind tunnel (1.75mx1.77m).

Figure 3.3 presents the variation of the measured and computed critical dynamic pressure when the Mach number increases from 0.7 to 0.9. The black curve is the measured result. Computational predictions rely on various tools with different accuracy.
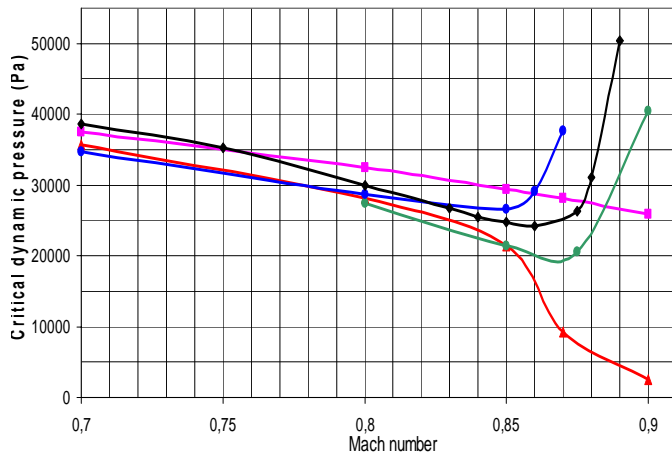

Fig. 3.3: Evolution of critical dynamic pressure between Mach 0.7 and Mach 0.9 (black: wind tunnel test, purple: Doublet Lattice Method, red: linearized Euler, blue: linearized NS, green: non linear unsteady NS)

The purple curve is obtained using the DLM. Results are quite accurate in the subsonic domain but, as expected, completely fail to predict the phenomena associated to the transonic domain. Linearized Euler results (red curve) are able to capture the initial drop in critical dynamic pressure as the Mach number increases, however a single degree of freedom instability appears beyond Mach=0.85. This instability can be related to the dynamics of the shock.

The linearized (blue curve) and nonlinear (green curve) Navier-Stokes results are in good agreement with the experimental results: both the initial drop and the sharp rise in critical pressure are captured when the Mach number increases. The single degree of freedom instability problem is solved. A discrepancy is still observed regarding the value of the Mach number associated to the rise in the critical pressure.

Identified benefits of the frequency domain linearized Euler and Navier-Stokes method can be summarized as follows:

- A more accurate description of the flow physics is achieved in the transonic domain due to the Euler or Navier-Stokes modelling (shocks in the transonic regime).
- The computation time is reduced by an order of magnitude compared to unsteady nonlinear computations.
- The frequency formulation of the problem allows a simple interfacing of the new method with the existing industrial flutter prediction process.

Shortcomings of the method include a lack of robustness of the linear solver especially for high Mach number computations. Also the need to linearize the turbulent models can be demonstrated. Work is in progress to address those needs.

4 DES for complex flows and loads

The DES approach makes it possible to predict very complex flows with large recirculation areas [11]. Its results can be used as an input to structural design (vibration, fatigue) provided that necessary interface tools are available.

4.1 Methodology

Two versions of the DES approach are currently used in the design process. The first approach is based on the Spalart-Allmaras model and the second on the k-ε SST two equations turbulence model.

The constants of both the Spalart and k-ε DES have been calibrated so that the far field models correctly reproduce the energy transfer. This calibration is performed using the Decay of Homogeneous Isotropic Turbulence test case. One difficulty associated to the DES approach is the behavior of the switch between the RANS model and the LES mode. In the near wall region the model should select the RANS mode. However, when the mesh is too fine in the longitudinal direction, the original DES approach will reduce the RANS viscosity. This

modeled stress depletion can yield flow separation. This phenomenon is usually called "Grid Induced Separation" (GIS). Near wall treatments have been proposed to avoid this problem [12]: DDES formulation is used for Spalart-Allmaras DES while Menter SST function is accurate for k-ε [11].

Examples of industrial applications include the design of weapon bays, compact curved air inlets, air brake attachment loads or the integration of engine reverses.

4.2 Prediction of loads in weapon bays

The design of weapon bays is one of the main challenges associated to the aerodynamic design of stealth aircraft. Large amplitude aerodynamic loads develop in an open bay leading to structural vibrations that could endanger the integrity of the aircraft. The sum of the so-called Rossiter modes and of the broad band noise associated with the shear layer creates extremely high vibration loads. Accurate aerodynamic predictions will avoid structural over-design with an associated weight penalty or reduced structural life due to fatigue [13].

A typical flow structure is illustrated in Figure 4.1. Complex vertical structures are observed.
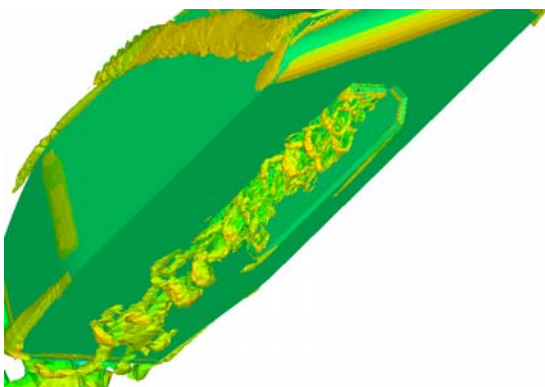

Fig. 4.1: flow in a weapon bay - snapshot of the vortex structures

The unsteady results produced by the DES computations are processed to define RMS loads, spectrum and cross correlation matrices for a range of frequencies in the selected areas where loads must be transferred to the Computational Structures Mechanics tools. It is well known that cross-correlation data tends to

converge slowly. An example of a comparison between experimental and DES cross correlation results is presented in Figure 4.2. Good agreement is observed and this validates the approach [13]. Experimental results were obtained in the large scale ONERA wind tunnel S1 Modane (section surface = 45m^2) in the transonic regime.
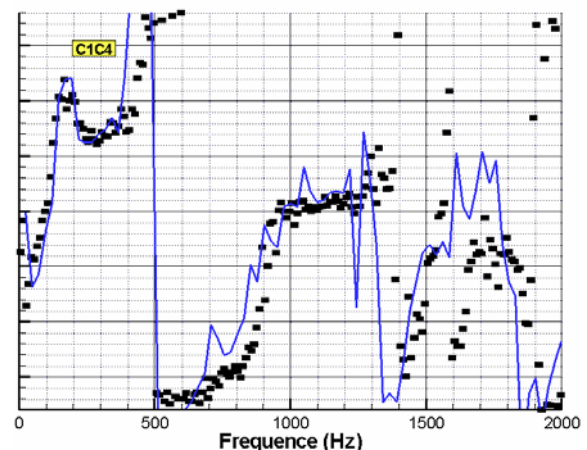

Fig. 4.2 : flow in a weapon bay - Correlation between two unsteady pressure signals - Experimental results: black dots, DES results: blue line

4.2 Application to airbrake loads

The design of airbrakes is a typical example of a design problem that extends beyond the prediction of the flow at cruise conditions. The complex flow features with large recirculation represents a challenge for turbulence models. RANS calculations are able produce a reasonably good prediction of the relative influence of the airbrake deflection on aircraft lift and drag. However unsteady efforts on the airbrake are not predicted. A DES computation was performed. A snapshot of the computed flow is presented on Figure 4.3.
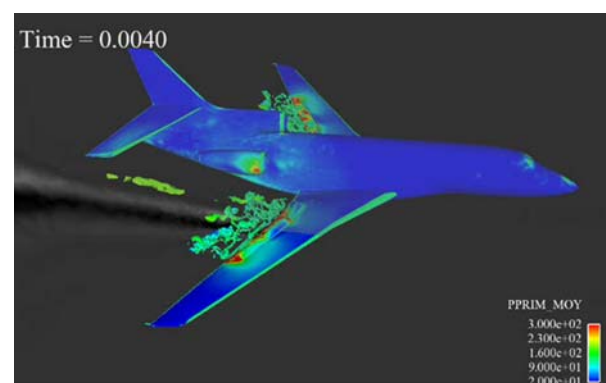

Fig. 4.3: flow around airbrakes

The DES simulation yields pressure spectrum along the surface that can be used for structural design.

One major challenge that must be addressed to extend the use of DES is the ability to deal with rather small recirculation areas associated to "moderate" curvature of the surface or "moderate" shock boundary layer interaction. Turbulence production in the transition zone is a key issue. Another issue is the reduction of the CPU requirements. Better LES models [14] and high order methods compatible with industrial use [22] will contribute to this objective.

5 Aeroacoustics

An increased emphasis is now set on the design of aircraft with reduced environment impact. This includes a low noise footprint. Recent development have been performed to allow an accurate evaluation of the acoustic performance of aircraft configurations [15].

5.1 Jet noise installation effects

Jet noise is the main contributor to aircraft noise at take-off. Increased shielding of engine noise can lead to innovative aircraft configuration as illustrated in Figure 5.1.
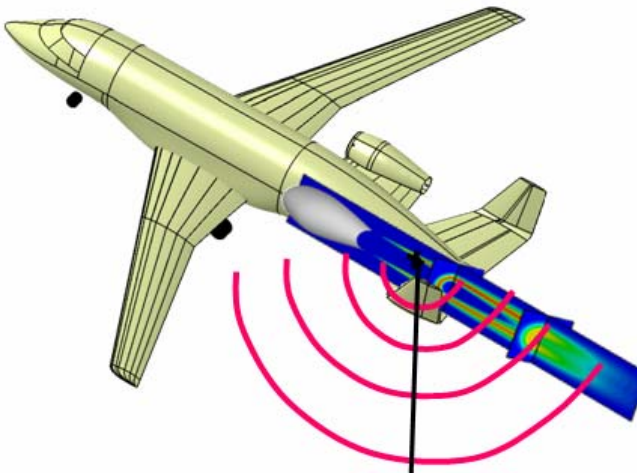

Fig. 5.1: Innovative configuration with engine noise shielding

The accurate assessment of the associated noise reduction is essential. A simulation process has been developed. A Navier Stokes computation with a two equations turbulence model is performed first. Turbulence data obtained from this computation are used as input to a noise source prediction tool based on Tam's model. As many as 10^5 sources are defined to achieve an accurate description of the noise generated by the jet. Noise propagation to the observation points in the far field is computed using a Boundary Element Method. This approach allows an accurate evaluation of the shielding by the airframe configuration. Since the number of sources is much higher than the number of observation points, an adjoint approach is very efficient.

This simulation process was validated in the framework of the EC funded NACRE project. Experimental testing was performed in the ONERA CEPRA 19 anechoic facility. Several configurations were considered. One example of an innovative configuration tested is presented on Figure 5.2. High lift devices are deployed.
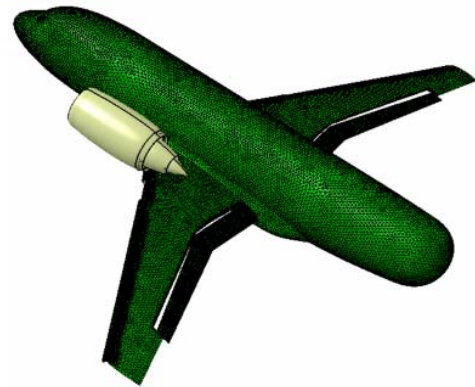

Fig. 5.2: Validation - NACRE configuration

Experimental (black line) and computed (blue line) results are compared on Figure 5.3 where the directivity at 2kHz is presented. A very good agreement is observed.
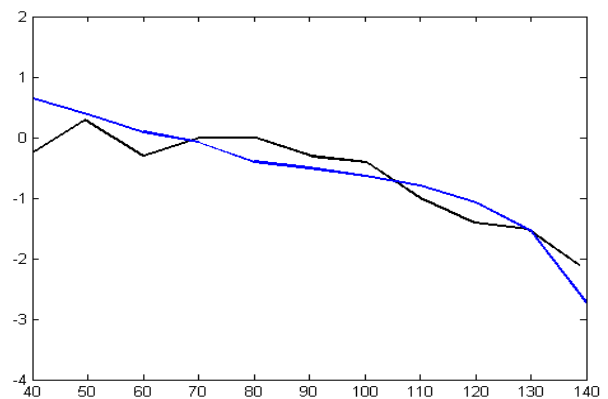

Fig. 5.3: Validation - NACRE configuration - Directivity at 2kHz (black: Anechoic wind tunnel test, Blue: computed results)

A simplified source model or a less accurate propagation tool would lead to a large degradation of the results.

5.2 Impact of aerodynamic flow on noise propagation

The impact of the aerodynamic flow on noise propagation can be significant when noise propagates through the jet. An example of a computation performed using a linearized Euler code is illustrated on Figure 5.4 where propagation of fan and turbine noise through a coaxial jet is computed.
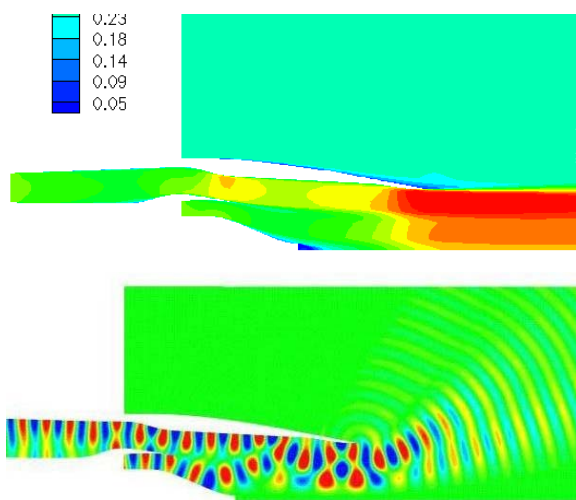

Fig. 5.4: Propagation of fan and turbine noise through the flow of a coaxial jet (top: Mach number, bottom: noise propagation predicted by linearized Euler)

6 Uncertainty quantification

The management of uncertainties is a rather new challenge for simulation-based aerodynamics [16], [17].

Uncertainty is an upper bound between the estimate of aircraft characteristics at a certain stage of its development and the actual characteristics of the aircraft once in service. Uncertainty is the consequence of both the quality of the means used during the development phase to estimate these characteristics and of the inaccurate knowledge of the final definition of the aircraft

6.1 Identification of sources of uncertainty

For a given aircraft definition, the ways to measure aerodynamic characteristics are

- Modelization, CFD,
- Wind Tunnel Testing,
- Flight Tests.

Each approach is associated to a certain accuracy of the estimated characteristics.

CFD uncertainties can have various origins.

The first source is the geometry considered for the computation : details are omitted, engine and bleeds are modelled, tolerance resulting from the manufacturing process are not included, aeroelastic deformation or icing are simplified.

Modelling hypothesis are still a prominent source of uncertainty, this includes mostly turbulence and transition modelling but also icing or thermochemical modelling.

Mesh quality is also a very large source of uncertainty especially for the more complex configurations.

Operating conditions are not perfectly known (weight of the aircraft, center of gravity).

Wind tunnel testing uncertainties include wind tunnel effect (tunnel walls, model support, flow homogeneity), mockup effect (size/ Reynolds number, transition, geometry simplification and inaccuracies, deformation, engine flow), accuracy of the instrumentation and measurement post processing.

Flight test uncertainties include the accuracy of evaluation of the thrust based on measurement of the fuel flow; the weight of the aircraft, its aeroelastic deformation, the location of its center of gravity and position of its control surfaces; the atmospheric conditions; the accuracy of the altitude and airspeed sensors and the tolerance resulting from the manufacturing process.

The evaluation of uncertainties associated to each measurement should be the result of a detailed and justified methodology. The treatment of uncertainties enables a rigorous management of performance engagements and associated risks.

6.2 Uncertainty quantification in CFD

Given an uncertainty on some input parameters of the CFD solver, our goal is to

quantify accurately the uncertainty of a quantity of interest (coefficient of drag or lift, for example). A known probability density function (PDF) is associated to each uncertain parameter. Methods are developed to propagate the uncertainty i.e. determine the impact of input uncertainty on the PDF of the output observation / quantity of interest.

Large-scale CFD simulations are considered. The number of uncertain input variables is rather small ($\approx 10\ldots$) and the number of output functions is even smaller ($\approx 1\ldots$).

Three methods can be considered to propagate uncertainties: the Monte Carlo method, the Polynomial Chaos approach and the Perturbation Method. These propagation methods will yield the four moments of the PDF (mean value, standard deviation, skewness and kurtosis). The PDF can be reconstructed from the four moments using Pearson's method, a key ingredient of the methodology.

The Monte Carlo method needs a reduced order model (response surface) otherwise the CPU cost would be too high. Since the design point is near optimal (i.e. gradients are close to zero) and also because of the non linear uncertainty propagation, second-order models are necessary. This requires the computation of 2nd-order derivatives for CFD models.

The Polynomial Chaos method considered is a non intrusive collocation approach, the main drawback of this approach is that the cost increases steeply with the number of unknown parameters.

The Perturbation Method requires 2nd order derivatives, it is a very efficient method even when the number of parameters increases.

Both the approximate Monte Carlo and the Perturbation Method rely on the computation of 2nd-order derivatives. A number of approaches with varying computational cost can be considered to compute these derivatives [18], [19]. The approach developed in [20] has been selected, it includes a formulation with two adjoint vectors associated to the flow variables and the mesh coordinates. The automatic differentiation tool TAPENADE [10] was used. The feasibility of this computation was demonstrated which constitutes a major development.

6.3 Examples

The benefit of the use of 2nd order derivatives is illustrated by two examples.

The first example is associated to a 3D generic fuselage configuration. Two variables are considered : the angle of attack and the side slip angle. The response surface corresponding to the variation of the pressure drag Cd with respect to those two variables is presented in Figure 6.1. The surface was defined using twenty five 3D Euler computations. The red curves are obtained with the 2nd order derivatives computed at one corner using the new CFD tools. A very good approximation of the response surface is obtained. First order derivatives are near zero at this point and a tangent plane would correspond to a constant Cd plane: this would be a rather poor approximation.
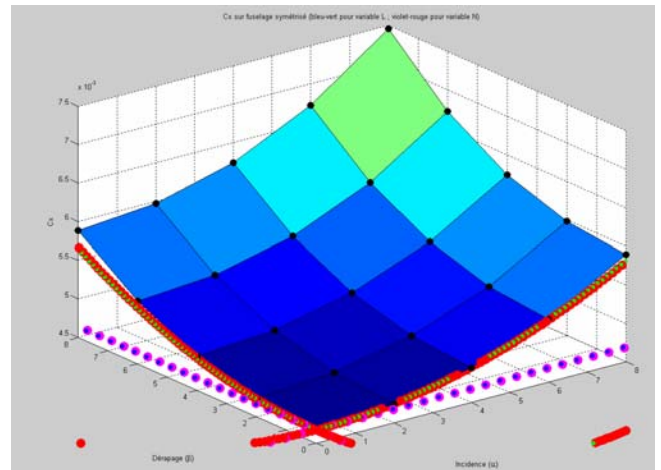

Fig. 6.1: Pressure Drag vs angle of attack and side slip angle, 3D Euler, generic fuselage

The second example considers as single parameter the trailing edge camber of the ONERA M6 wing. This geometric feature is illustrated on Figure 6.2.
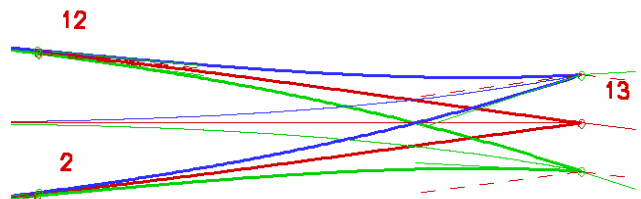

Figure 6.2: Trailing Edge Camber

The variation of drag with this parameter is presented in Figure 6.3. The reference curve is

obtained by several non linear computations (blue curve). The result obtained using 1st order derivatives is the tangent green curve. 2nd order derivatives are used to obtain the red curve, the accuracy of this approximation is obvious.
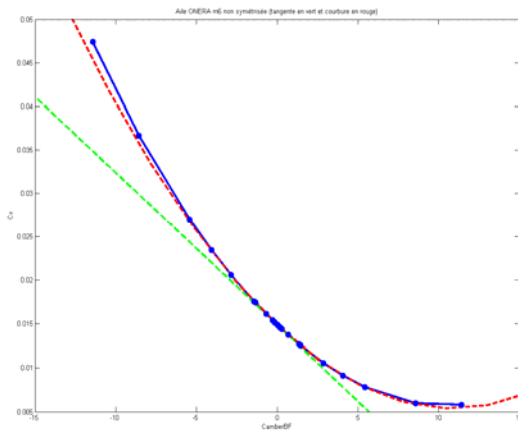

Fig. 6.3: Pressure Drag vs Trailing Edge Camber, 3D Euler, ONERA M6 wing

If the camber is assumed to be an uncertain parameter the drag coefficient becomes an uncertain aerodynamic output of the Euler computation. The probability density function (PDF) can be obtained using a propagation method. The PDF is presented in Figure 6.4.
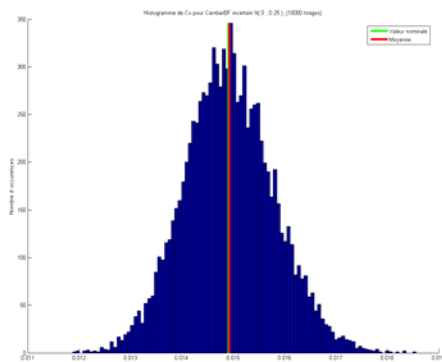

Fig. 6.4: Probability density function for the drag coefficient C_D, uncertain Trailing Edge camber, PM order 2, CoV=5.85%

This illustrates the ability to propagate uncertainty.

6.4 Uncertainty quantification - conclusion

When the number of uncertain parameters is low, the non-intrusive Polynomial Chaos method with five collocation points is recommended. The Perturbation Method replaces the non-intrusive Polynomial Chaos

when the number of parameters is above 3~4. This technique is feasible thanks to a breakthrough in the ability to compute 2nd order derivatives. The main shortcoming is the lack of accuracy of the computed derivatives for the more complex turbulent flows (high transonic flows, strong shock-boundary layer interactions). It is possible to explain this deficiency by the "frozen" turbulence hypothesis. Turbulence models are now being differentiated and preliminary results are encouraging.

7 Conclusions

Key recent developments that impact simulation-based design have been reviewed and illustrated. A number of major trends that have not been discussed can be identified :

- Multi-disciplinary Design Optimization is a main target. Relevant strategies and required methods are progressively put into place.
- Integrated design environments are implemented to greatly increase the efficiency of the simulation-based design process.
- New High Performance Computers bring constant challenges to existing design tools: multiprocessor / multicore architectures with a mix of distributed and shared memory and GPU accelerated cores will bring new capabilities if relevant implementations can be found.
- High order methods will be the kernel of a new generation of CFD codes [21], [22] that will provide a new level of accuracy.
- Better transition models is an example of a critical simulation capability that will be key to the design of new fuel efficient laminar aircraft. Recent models include intermittency transport models [23].

References

[1] Jameson A. Aerodynamics. *Encyclopedia of Computational Mechanics, Volume 3*. Wiley 2004.

[2] Chalot F. Industrial Aerodynamics, *Encyclopaedia of Computational Mechanics, Vol. 3*. Wiley, 2004.

[3] Rossow C, Cambier L. European numerical aerodynamics simulation systems. *100 Volumes of NNFM and 40 years of numerical fluid mechanics*, Springer, 2009.

[4] Rostand P. New generation aerodynamic and multidisciplinary design methods for FALCON business jets. Application to the F7X, AIAA paper 2005-5083, 23rd AIAA Applied Aero Conference, 2005.

[5] Herskovits J, Laporte E, Le Tallec P and Santos P. "A Quasi-Newton Interior Point Algorithm applied for constrained optimum design in computational fluid dynamics", *European Journal of Finite Elements*, Vol.5, pp 595–617, Hermes, 1996.

[6] Kleinveld S, Rogé G, Daumas L and Dinh Q. Differentiated parametric CAD used within the context of automatic aerodynamic design optimization, AIAA paper 2008-1308.

[7] Alauzet F, Borel S, Daumas L, Dervieux A, Dinh Q, Kleinveld S, Loseille A, Mesri Y, Rogé G. "Multimodel design strategies applied to sonic boom reduction", REMN 17-2008, Shape design in aerodynamics, pages 245 to 269, 2008.

[8] Fanion T. Étude de la simulation numérique des phénomènes d'aéroélasticité dynamique: Application au problème du flottement des avions, Ph.D. thesis, Université Paris Dauphine, September 2001.

[9] Daumas L, Chalot F, Forestier N and Johan Z. Industrial use of linearized CFD tools for aeroelasic problems, IFASD 2009-054, 2009.

[10] Hascouet L, Dervieux A and Pascual V. "Software TAPENADE INRIA 2002, versions 2.0 and later hereinafter 'the software' ", developed by TROPICS project at INRIA Sophia Antipolis.

[11] Chalot F, Levasseur V, Mallet M, Petit G, Reau N. LES and DES simulations for aircraft design, AIAA paper 2007-0723, 2007.

[12] Spalart P R, Deck S, Shur M L, Squires K D, Strelets M, Travin A. "A new version of Detached Eddy Simulation resistant to ambiguous grid densities", *Th. And Comp. Fluid Dyn*.

[13] Daumas L, Chalot F, Levasseur V, Mallet M, Reau N. LES and DES aeroacoustics simulations for inflight open weapon bay, IFASD 2009-099, 2009.

[14] Levasseur V, Sagaut P, Chalot F, Davroux A. "An entropy variable based VMS/GLS method for the simulation of compressible flows on unstructured grids", *Computer methods in applied Mechanics and Engineering,* 195, 1154-1179, 2006.

[15] Barre S, Lemaire S, Daumas L, Levasseur V. Prédiction des effets de l'installation motrice sur le bruit généré par un avion d'affaires. AAAF 41-19, 2008.

[16] Herbin H, Jakubowski J, Ravachol M and Dinh Q. Management of uncertainties at the level of global design and methodologies to obtain CFD results, NATO-RTO-MP-AVT-147, A75, 2007.

[17] Hirsch C and al. NODESIM-CFD: Non deterministic simulation for CFD based design methodologies, European Sixth Framework Program, AST5-CT-2006-030959, http://www.nodesim.eu, 2006.

[18] Ghates D, Giles M B. Efficient Hessien calculation using Automatic Differentiation, no 2007-4059, AIAA 25th Applied Aero conference, 2007.

[19] Martinelli M. Sensitivity evaluation in aerodynamic optimal design, Ph D Thesis, Scuola Normale Superior - Université de Sophia Antipolis, 2007.

[20] Martin L. "Conception aérodynamique robuste", PhD Thesis, University of Toulouse, June 30th 2010.

[21] Kroll N, Bieler H, Deconinck H, Couallier V, van der Ven H, and Sørensen K. ADIGMA - A European Initiative on the Development of Adaptive Higher-Order Variational Methods for Aerospace Applications. NNFM, Vol 230, Springer, 2010.

[22] Chalot F, Normand P.E. Towards high fidelity industrial CFD. 5th ECCOMAS CFD conference, paper 01440, 2010.

[23] Menter F R, Langtry R, Likki SR, Suzen Y B, Huang P G, Volker S. A correlation based transition model using local variables. J. of Turbomachinery 128, 2006.

Frederic.Chalot@Dassault-Aviation.com
Michel.Mallet@Dassault-Aviation.com
Gilbert.Roge@Dassault-Aviation.com

Acknowledgement

Copyright Statement